# Multiple Hydrophone Arrays based Underwater Localization with Matching Field Processing

Shuo Jin, Xiukui Li
School of Information and Communication Engineering
Dalian University of Technology

***Abstract*—Matched field processing technology (MFP) is a general passive localization method for underwater sound source due to its advantages in ultra-long distance positioning. In this paper, assume the total number of hydrophones remains unchanged, a single hydrophone array is divided into multiple hydrophone sub-arrays for independent positioning, and the positioning results of sub-arrays are fused to reduce the impact of noise and improve the robustness of the positioning system. Based on the traditional Bartlett processor, we derive the formula for average positioning error which varies with signal to noise ratio (*SNR*) and the number of hydrophones. The formula is used to decide the optimal structure of sub-arrays, i.e., the number of sub-arrays and the number of hydrophones in each sub-array. Experiments and simulations proves that multiple sub-arrays can improve the positioning accuracy compared with the single hydrophone array in the noisy environment. The average positioning errors produced by the experiments are consistent with the numerical ones based on the theoretical analysis.**

***Keywords*—Matched Field Processing (MFP); hydrophone array; source localization; underwater acoustic**

## I. Introduction

After decades of development, underwater acoustic positioning technology is the primary means for underwater positioning and tracking in various applications and fields. Underwater positioning can be divided into active and passive positioning. Active positioning usually can be categorized into three basic techniques: ultra short baseline location (USBL), short baseline location (SBL) and long baseline location (LBL). Those techniques can be combined to create complex positioning system including long ultra short baseline location (LUSBL) and short and long ultra short baseline location (SLUSBL), etc. Passive positioning implements the positioning by processing noise or signal generated by the target source without actively generating wave; thus it can achieve high concealment. Passive positioning mainly includes four methods: ternary method, target motion analysis (TMA), matched field processing (MFP) and focused beamforming. In various underwater positioning methods, MFP takes advantages of the characteristics of acoustic field propagation to obtain the source position, and it is an important means of underwater long-distance positioning, particularly for ultra long distance positioning.

Matched field processing technology is a general means of underwater passive positioning due to its advantages in ultra-long distance positioning. Considering the marine environment parameters and acoustic communication channel characteristics, MFP estimates the acoustic field amplitude and phase of receive array by using the underwater acoustic field model. The amplitude and phase estimates form replica vectors which is matched with receiving data in hydrophone arrays. This realizes the passive positioning of underwater targets and accurate estimation of marine environmental parameters.

The waveguide propagation theory is applied to underwater acoustic propagation analysis by Clay in 1966 [1], and it is widely used in MFP [2–6]. The positioning error are mainly produced by environmental mismatch and underwater noise. Inaccurate environmental parameters will cause errors in sound field calculation, resulting in positioning errors [7–11]. When the noise power is high, the signal to noise ratio(*SNR*) of the receiving signal will reduce, and the positioning error will increase. Debever *et al.* designs a coherent wide-band white noise constrained processor to reduce the effect of noise on the positioning [12]. Collins *et al.* proposes a processor to eliminate the noise in the signal [13]. Lee *et al.* investigates a robust adaptive positioning algorithm used in shallow water [14]. Seong *et al.* designs an optimal processor for motion source localization with correlation noise based on the normal mode propagation mode [15].

Single array MFP is evolving into multiple array MFP. Nicholas *et al.* studies the performance of coherent and incoherent positioning with underwater L-shaped array which consists of a horizontal and a vertical array. The results show that coherent and incoherent positioning results are not of much difference [16]. Zurk *et al.* uses the received signals at three vertical arrays in Santa Barbara Channel Experiment (SBCX) to localize the mobile source with known motion information which is obtained through adaptive MFP algorithm [17]. Tollefsen *et al.* designs three different processors for multi-array MFP, and proves that coherent processor can achieve the best performance when the synchronization error is small [18].

The design of hydrophone array involves multiple aspects. Tracey *et al.* discusses the prediction of the sidelobe level of matched results in conventional MFP, and proposes a method to analyze and predict the relationship between the output power distribution of traditional MFP fuzzy surface and array aperture [19]. Bogart *et al.* investigates the MFP performance of several horizontal line array apertures and compares to a full water column vertical array in a simulated range-independent shallow water environment [20]. It is demonstrated that a horizontal array of sufficient length can equal or exceed the water column vertical array in range–depth localization performance. Tantum *et al.* proposes a general guideline for designing matched field processing arrays using normal mode propagation model, and evaluates the performance of various line array configurations [21].

Compared with single array, multiple sub-arrays structure can improve the robustness of the localization system in dealing with environment mismatch and large noise. Due to sound directivity, if only one array is used for positioning, the positioning result may have a large error when the array is located at the direction where the received sound signal is with low energy. However, when multiple arrays are used, certain arrays may be in the direction where the received sound signal is with high energy even if some arrays are receiving low-power signals. The underwater white noise can be considered almost equal at different positions. We use the received *SNR* as the weighting coefficient in the final positioning result fusion, and the positioning error will be reduced. When the power of the sound source is low which yields a low received *SNR*, the positioning accuracy yielded by multiple arrays is higher than that of single array.

In this paper, we propose multiple sub-arrays joint positioning method. Assume the total number of hydrophones remains unchanged, a single hydrophone array is divided into multiple hydrophone sub-arrays for independent positioning, and the positioning results of sub-arrays are fused to obtain the sound source location. This will reduce the impact of noise and improve the robustness of the positioning system. Based on the traditional Bartlett processor, we derive the formula for average positioning error which varies with *SNR* and the number of hydrophones. The formula is used to decide the optimal structure of sub-arrays, i.e., the number of sub-arrays and the number of hydrophones in each sub-array. Experiments and simulations proves that multiple sub-arrays can improve the positioning accuracy compared with the single hydrophone array in the noisy environment. The average positioning errors produced by the experiments are consistent with the numerical ones based on the derived formula.

The remainder of this paper is organized as follows. Section II introduces the system model of traditional MFP and the signal propagation model. In Section III, the positioning principle of multiple sub-arrays are introduced. In Section IV, the formula that the average positioning error varies with different hydrophone allocation methods is derived. Section V presents the performance of multiple sub-arrays joint positioning by underwater real data and simulations, and Section VI concludes this paper.

## II. System Model

Matching field processing is a general technology for long-distance underwater positioning. Its principle is to match the actual signal received by hydrophones with the acoustic field which is calculated at the position of hydrophone array. The position with the largest matching result is considered to be where the sound source is located.

The matching result of traditional processor is the power weighted sum of each hydrophone,

$$\boldsymbol{B_a}\left(\boldsymbol{x}\right)=\frac{1}{L}\sum_{l=1}^{L}\left|\boldsymbol{W}\left(\boldsymbol{x},l\right)^{H}\boldsymbol{Y}\left(\boldsymbol{x_R},l\right)\right|^{2} \tag{1}$$

where $L$ is the number of segments selected for matching at the receiving hydrophone; $\boldsymbol{x}=(r,h)$ is the position point to be matched, where $r$ is the horizontal distance between the sound source and the array, and $h$ is the depth of the sound source, $\boldsymbol{W}(\boldsymbol{x},l)=\frac{\boldsymbol{G}(\boldsymbol{x},l)}{|\boldsymbol{G}(\boldsymbol{x},l)|}$ is the weight of the sound pressure calculated by using the underwater acoustic channel model, where $\boldsymbol{G}(\boldsymbol{x},l)=(g_1(\boldsymbol{x},l),g_2(\boldsymbol{x},l),...g_N(\boldsymbol{x},l))^H$. $g_i(\boldsymbol{x})$ is the sound pressure received by the $i$th hydrophone when the sound source transmits the signal in unit power, and $N$ is the number of hydrophones. $\boldsymbol{Y}(\boldsymbol{x_R},l)$ is the actual received signal,

$$\boldsymbol{Y}(\boldsymbol{x_R},l)=(1+J)P_s\boldsymbol{G}(\boldsymbol{x_R},l)+\boldsymbol{T} \tag{2}$$

where $J$ is the attenuation factor of the acoustic signal in the propagation channel; $P_s$ is the power of the source; $\boldsymbol{x_R}$ represents the sound source position. $\boldsymbol{T}$ is the additive white Gaussian noise, and $T=(N_1(\mu_1,\sigma_1^2),N_2(\mu_2,\sigma_2^2),...N_N(\mu_N,\sigma_N^2))^H$. It can be considered that the additive noise in each hydrophone follows the same Gaussian distribution $N(\mu,\sigma^2)$, where $\mu$ can be regarded as 0.

In the actual marine environment, the underwater noise may be large, and when the transmitting power of the sound source is low, the *SNR* at the receiver will be low. In addition, most underwater sound sources are mobile, and the transmission power of the source in a certain direction is high, and it is low in other directions. Therefore, when the sound source is in the moving state, if the sound wave propagation direction of the source changes, the *SNR* of some positions at the receiver may reduce, which may result in serious deviation of the positioning result.

In this situation, dividing a single array into multiple independent arrays and implementing jointly localization will improve the positioning accuracy. When the hydrophone arrays are placed in different positions, the hydrophone arrays with low *SNR* will be assigned a lower weight in deciding the location of sound source. This will reduce the environment influence, particularly in low *SNR* scenario, and improves the fault tolerance of the system.

## III. Multiple Sub-arrays Joint Location

Compared with the single array, the advantage of multiple sub-arrays joint localization is its strong adaptability in the complex and varied underwater environments. When the sound source radiates the sound wave outward in the free field, the sound pressure level presents an uneven property with different directions, which is called the directivity of the sound source. The directivity of the sound source is related to the scale of the sound source and the radiation wavelength. When the sound source is small enough to be regarded as the point sound source, the sound wave diverges evenly outward in the form of approximately spherical surface with the sound source as the center. Thus, the sound pressure levels are equal at the points which are of equal distances to the source center. When the scale of the sound source is much larger than the wavelength of the sound wave, the sound wave propagates in a concentrated direction in the form of a sound beam, the sound wave can be considered to have strong directivity. Therefore, for this kind of sound source, the horizontal distribution range of multiple sub-arrays is wider, and it is easier to realize the full utilization of acoustic signal.

The system model and array structure of multiple sub-arrays based positioning are shown in Fig. 1 and Fig. 2 respectively. $Ar_i$ is the $i$th array.

In the proposed positioning system, we can adopt different positioning methods for different arrays (see Fig. 1). The specific method can be determined according to the noise intensity and the environments where the arrays are situated. Finally, the positioning results of different arrays are averaged with different weights which will be determined by the number of hydrophones and noise intensity of each array.

Assume $N$ hydrophones are available. Those $N$ hydrophones are divided into $m$ groups, and each group has $\frac{N}{m}$ hydrophones, called sub-array (see Fig. 2). Different sub-arrays can be placed in different positions according to the actual environment to form a spatial pattern, and the distance between different arrays is set accordingly. The vertical positions of different sub-arrays can be different. The horizontal distance between each sub-array and the sound source is denoted by $r_i, i = 1, 2, \cdots, m$. The $m$ hydrophone sub-arrays are used to localize the sound source independently, and the location results produced by $m$ sub-arrays are fused to determine the location of sound source. Take one array as the reference array, such as $Ar_1$. Assume that the horizontal distance between $Ar_i$ and $Ar_1$ is $s_i$, and the positioning result of the $i$th array is denoted by $(r_i, h_i)$, where $h_i$ is the depth of the sound source obtained by the $i$th sub-array. Then the final sound source location is

$$\begin{aligned} r_1 &= \boldsymbol{\Omega} \cdot \boldsymbol{R} \\ h_1 &= \boldsymbol{\Omega} \cdot \boldsymbol{H} \end{aligned} \tag{3}$$

where

$$\begin{aligned} \boldsymbol{\Omega} &= (\omega_1, \omega_2, ...\omega_m) \\ \boldsymbol{R} &= (r_1 - s_1, r_2 - s_2, ...r_m - s_m)^T \\ \boldsymbol{H} &= (h_1, h_2, ...h_m)^T \end{aligned} \tag{4}$$

where $\omega_i$ represents the weight of the $i$th sub-array. Hence, when the position of $Ar_1$ is known, the distance and depth between the sound source and $Ar_1$ can be inferred.

In Fig. 2, when the sound source is in some directions, due to the spatial structure of multiple arrays, the receiving power of the sound source signal at the array will be increased and the received *SNR* can be improved.

The challenging work for the multiple sub-arrays joint localization includes techniques of forming the hydrophone array pattern, weight assignment of different hydrophones array, and synchronization of array hydrophones.

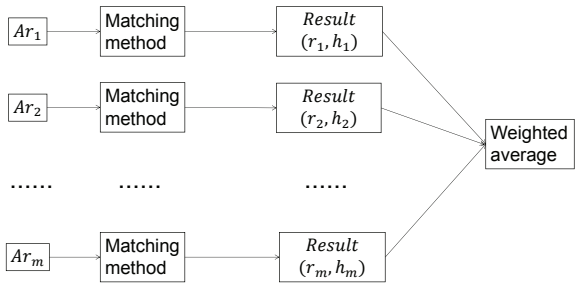


Fig. 1. System Model.

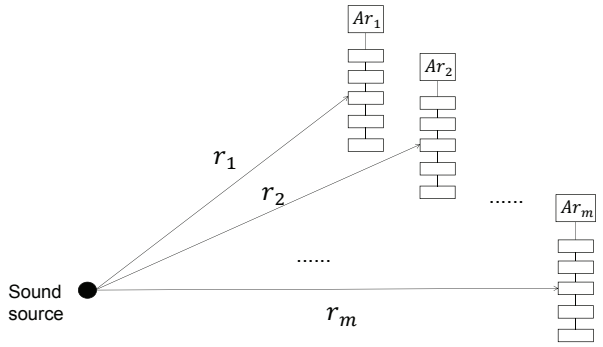


Fig. 2. Array Structure.

## IV. Distribution of Hydrophone Array and Performance Analysis

If $l$ is set as a constant value, then (2) can be written as

$$\boldsymbol{Y}(\boldsymbol{x_R}) = (1 + J)P_s\boldsymbol{G}(\boldsymbol{x_R}) + \boldsymbol{T} \tag{5}$$

To analyze the influence of different parameters on the matching results, function $F(\boldsymbol{x})$ is assumed to be the product of $\boldsymbol{W}(\boldsymbol{x})$ and $\boldsymbol{Y}(\boldsymbol{x_R})$.

$$\begin{aligned} F(\boldsymbol{x}) &= \boldsymbol{W}(\boldsymbol{x})^H \boldsymbol{Y}(\boldsymbol{x_R}) \\ &= (1 + J)P_s \sum_{i=1}^{N} \frac{g_i(\boldsymbol{x_R})g_i(\boldsymbol{x})}{\sqrt{\sum_{k=1}^{N} g_k^2(\boldsymbol{x})}} + n \sum_{i=1}^{N} \frac{g_i(\boldsymbol{x})}{\sqrt{\sum_{k=1}^{N} g_k^2(\boldsymbol{x})}} \end{aligned} \tag{6}$$

where $n$ follows the normal distribution $\mathcal{N}(0, \sigma^2)$.

From (6), for each $\boldsymbol{x}$, $F(\boldsymbol{x})$ is a normal distribution. Its mean is $(1 + J)\sum_{i=1}^{N} \frac{g_i(\boldsymbol{x_R})g_i(\boldsymbol{x})}{\sqrt{\sum_{k=1}^{N} g_k^2(\boldsymbol{x})}}$, and variance is $\sigma^2 \sum_{i=1}^{N} \frac{g_i(\boldsymbol{x})}{\sqrt{\sum_{k=1}^{N} g_k^2(\boldsymbol{x})}}$, where $(1 + J)P_s$ is a constant value and can be set as $k$.

Let

$$M(\boldsymbol{x}) = k \sum_{i=1}^{N} \frac{g_i(\boldsymbol{x_R})g_i(\boldsymbol{x})}{\sqrt{\sum_{k=1}^{N} g_k^2(\boldsymbol{x})}} \tag{7}$$

be the mean of $F(\boldsymbol{x})$ and it is a function of position $\boldsymbol{x}$.

From (7),

$$\frac{M(\boldsymbol{x})}{\sqrt{\sum_{k=1}^{N} g_k^2(\boldsymbol{x}_R)}} = k \sum_{i=1}^{N} \frac{g_i(\boldsymbol{x_R})g_i(\boldsymbol{x})}{\sqrt{\sum_{k=1}^{N} g_k^2(\boldsymbol{x}_R)}\sqrt{\sum_{k=1}^{N} g_k^2(\boldsymbol{x})}} \tag{8}$$

Obviously, (8) is the formula for calculating the cosine value between two vectors. Thus when $\boldsymbol{x} = \boldsymbol{x}_R$, $\frac{M(\boldsymbol{x})}{\sqrt{\sum_{k=1}^{N} g_k^2(\boldsymbol{x}_R)}}$ has the maximum value of $k$. $\sqrt{\sum_{k=1}^{N} g_k^2(\boldsymbol{x}_R)}$ is a constant value. Hence $M(x)$ has a maximum value of $k\sqrt{\sum_{k=1}^{N} g_k^2(\boldsymbol{x}_R)}$ at $\boldsymbol{x} = \boldsymbol{x}_R$. The value of $M(\boldsymbol{x})$ is related to $N$; thus $M(\boldsymbol{x})$ can be written as $M(\boldsymbol{x}, N)$. Then the value of $F(\boldsymbol{x})$ is also related

to $N$.

$$F(\boldsymbol{x}, N) = M(\boldsymbol{x}, N) + n \sum_{i=1}^{N} \frac{g_i(\boldsymbol{x})}{\sqrt{\sum_{k=1}^{N} g_k^2(\boldsymbol{x})}} \tag{9}$$

For each position $\boldsymbol{x}$, $F(\boldsymbol{x}, N)$ is a Gaussian distribution with mean $M(\boldsymbol{x}, N)$ and variance $\sigma^2 \sum_{i=1}^{N} \frac{g_i(\boldsymbol{x})}{\sqrt{\sum_{k=1}^{N} g_k^2(\boldsymbol{x})}}$. In the calculation of the variance, $N$ appears in both the numerator and denominator. However it is obvious that the values of the numerator and denominator do not increase in proportion with the increase of $N$; thus the value of variance is also related to $N$, which can be written as $\sigma^2(\boldsymbol{x}, N)$.

Set a total of $d$ location points on the ambiguity surface. Denote the probability that point $\boldsymbol{x}_t (1 \leq t \leq d)$ can reach the maximum value by $\mathbb{P}_t(\boldsymbol{x}_t, N)$ and the absolute distance between the potential location point and the true position by $|\boldsymbol{x}_t - \boldsymbol{x}_R|$. The positioning error of $\boldsymbol{x}_t$ is defined as $\mathbb{P}_t(\boldsymbol{x}_t, N) \times |\boldsymbol{x}_t - \boldsymbol{x}_R|^2$ if point $\boldsymbol{x}_R$ is considered as the position of the sound source.

The average positioning error can be given by

$$E(N) = \frac{\sum_{t=1}^{d} \mathbb{P}_t(\boldsymbol{x}_t, N) \times |\boldsymbol{x}_t - \boldsymbol{x}_R|^2}{d} \tag{10}$$

For the position point $\boldsymbol{x}_t$, the value of $F(\boldsymbol{x}_t, N)$ follows the Gaussian distribution. Hence $(\bar{\boldsymbol{x}} - 3\sigma(\boldsymbol{x}_t, N), \bar{\boldsymbol{x}} + 3\sigma(\boldsymbol{x}_t, N))$ can be considered as the range of $F(\boldsymbol{x}_t, N)$, where $\bar{\boldsymbol{x}}$ is the mean of $F(\boldsymbol{x}_t, N)$, i.e., the value of $M(\boldsymbol{x}_t, N)$. Hence the Euclidean distance between the mean of $F(\boldsymbol{x}, N)$ and $F(\boldsymbol{x}_R, N)$ is $|M(\boldsymbol{x}_R, N) - M(\boldsymbol{x}_t, N)|$.

To find $\mathbb{P}_t(\boldsymbol{x}_t, N)$, the continuous probability density function is discretized. We can divide the possible values of $F(\boldsymbol{x}_t, N)$ into $\alpha (\alpha \in \mathbb{N}^*)$ segments, where $\mathbb{N}^*$ represents the set of positive integers. The length of each segment is denoted by $\beta$, and $\beta = \frac{6\sigma^2(\boldsymbol{x}_t, N)}{\alpha}$. Therefore, the probability that $F(\boldsymbol{x}_t, N)$ reaches the maximum is the sum of the probabilities of all segments of $F(\boldsymbol{x}_t)$ reaching the maximum. Let the start and end values of segment $i$ of $F(\boldsymbol{x}_t, N)$ be $C_i(\boldsymbol{x}_t, N)$ and $C_{i+1}(\boldsymbol{x}_t, N)$, respectively. Then

$$\begin{aligned}
\mathbb{P}_t(\boldsymbol{x}_t, N) &= \mathbb{P}(F_{max}(\boldsymbol{x}, N) = F(x_t, N)) \\
&= \sum_{i=1}^{\alpha-1} \mathbb{P}(F_{max}(\boldsymbol{x}, N) \in (C_i(\boldsymbol{x}_t), C_{i+1}(\boldsymbol{x}_t))) \\
&= \sum_{i=1}^{\alpha-1} \frac{\prod_{j=1}^{d} \mathbb{P}(L_1(i,j,t) | L_2(i,t))}{\mathbb{P}(F(\boldsymbol{x}_t, N) < C_i(\boldsymbol{x}_t, N))}
\end{aligned} \tag{11}$$

where $L_1(i,j,t)$ represents $F(\boldsymbol{x}_j, N) < C_i(\boldsymbol{x}_t, N)$, and $L_2(i,t)$ represents $F(\boldsymbol{x}_t, N) \in (C_i(\boldsymbol{x}_t, N), C_{i+1}(\boldsymbol{x}_t, N))$. $L_1(i,j,t)$ and $L_2(i,t)$ are independent of each other, then

$$\begin{aligned}
\mathbb{P}(F_{max}(\boldsymbol{x}, N) &= F(\boldsymbol{x}_t, N)) \\
&= \sum_{i=1}^{\alpha-1} \frac{\prod_{j=1}^{d} \mathbb{P}(L_1(i,j,t)) \mathbb{P}(L_2(i,t))}{\mathbb{P}(F(\boldsymbol{x}_t, N) < C_i(\boldsymbol{x}_t, N))} \\
&= \sum_{i=1}^{\alpha-1} \frac{\prod_{j=1}^{d} A_1(\boldsymbol{x_t}, i, j) A_3(\boldsymbol{x}_t, i)}{A_2(\boldsymbol{x}_t, i)}
\end{aligned} \tag{12}$$

where

$$A_1(\boldsymbol{x}_t, i, j) = \int_{-3\sigma^2(\boldsymbol{x}_j, N)}^{C_i(\boldsymbol{x}_t)} f(M(\boldsymbol{x}_j, N), \sigma(\boldsymbol{x}_j, N)) dz \tag{13}$$

$$A_2(\boldsymbol{x}_t, i) = \int_{-3\sigma^2(\boldsymbol{x}_t, N)}^{C_i(\boldsymbol{x}_t)} f(M(\boldsymbol{x}_t, N), \sigma(\boldsymbol{x}_t, N)) dz \tag{14}$$

$$A_3(\boldsymbol{x}_t, i) = \int_{C_i(\boldsymbol{x}_t)}^{C_{i+1}(\boldsymbol{x}_t)} f(M(\boldsymbol{x}_t, N), \sigma(\boldsymbol{x}_t, N)) dz \tag{15}$$

where $f(\mu, \xi)$ represents the probability density function of normal distribution $\mathcal{N}(\mu, \xi)$. If the maximum value $M(\boldsymbol{x}_k, N) + 3\sigma^2(\boldsymbol{x}_K, N)$ of point $\boldsymbol{x}_k$ is not greater than the minimum value $C_i(\boldsymbol{x}_t, N)$ of segment $i$, then the $\mathbb{P}_k(\boldsymbol{x}_k, N)$ is considered to be 0. Therefore, for each potential location point, the smaller the $\sigma(\boldsymbol{x}_t, N)$ is, the larger the distance between $M(\boldsymbol{x}_t, N)$ and $M(\boldsymbol{x}_R, N)$ is. This means the a smaller positioning error will be produced, particularly for the position points close to the true position of the sound source.

Because the matching result information of all other location points need to be considered when calculating the probability that a location point obtain the maximum value of matching result, the computational complexity of this method increases with the number of location points to be matched. Therefore, in the actual positioning process, if there are many location points to be matched, the following simple method can be used to calculate $\mathbb{P}_t(\boldsymbol{x}_t, N)$.

Interval $(u_1, u_2)$ can be regard as the value range of $F(\boldsymbol{x}, N)$ at the true position point $\boldsymbol{x}_R$, where $u_1 = M(\boldsymbol{x}_R, N) - 3\sigma^2(\boldsymbol{x}_R, N)$ and $u_2 = M(\boldsymbol{x}_R, N) + 3\sigma^2(\boldsymbol{x}_R, N)$. Therefore, for the position point $\boldsymbol{x}_t$, $\mathbb{P}_t(\boldsymbol{x}_t, N)$ can be approximately expressed by the integral of the probability density function of $F(\boldsymbol{x}_t, N)$ in the interval $(u_1, u_2)$,

$$\begin{aligned}
\mathbb{P}_t(\boldsymbol{x}_t, N) &= \mathbb{P}_e(F_{max}(\boldsymbol{x}, N) = F(\boldsymbol{x}_t, N)) \\
&= \int_{u_1}^{u_2} \frac{1}{\sqrt{2\pi}\sigma(\boldsymbol{x}_t, N)} exp\left(-\frac{(z - M(\boldsymbol{x}_t, N))^2}{2\sigma^2(\boldsymbol{x}_t, N)}\right) dz
\end{aligned} \tag{16}$$

The positioning accuracy can be expressed as the reciprocal of the mean error,

$$Q(N) = \frac{1}{E(N)} = \frac{1}{\sum_{t=1}^{d} \mathbb{P}_t(\boldsymbol{x}_t, N) \times |\boldsymbol{x}_t - \boldsymbol{x}_R|^2} \tag{17}$$

The positioning results of all arrays will be averaged with weights. A hydrophone array will be divided into multiple hydrophone sub-arrays. If the total number of hydrophones remains unchanged, the number of hydrophones in each hydrophone sub-array will decrease. Assume there are $N$

hydrophones and $m$ hydrophone sub-arrays. The number of hydrophones in the $i$th hydrophone sub-array is denoted by $N_i$; thus $N = \sum_{i=1}^{m} N_i$. The weight coefficient depends on the *SNR* and the number of hydrophones at each receiving sub-array. The weight coefficient increases with the *SNR*. If the received signal power is $P_r$ and the noise power is $P_n$ at each sub-array, the signal-to-noise ratio is $SNR = \frac{P_r - P_n}{P_n}$.

Thus $Q(N, m, SNR)$ definition

$$Q(N, m, SNR) = \frac{\sum_{i=1}^{m} \omega_i Q_i}{m} \tag{18}$$

where

$$\omega_i = \frac{SNR_i \times N_i}{\sum_{k=1}^{m} SNR_k \times N_k} \tag{19}$$

Therefore, when the noise power at the receiving array is known, the signal power can be obtained by subtracting the noise power from the received signal power, and then the positioning error can be calculated by (18). When the actual *SNR* of the received signal is small, the optimal number of hydrophones can be determined to improve the positioning accuracy by calculating the positioning error of the array.

## V. Marine Data Processing and Simulation Experiment

### A. Experimental Environment

The environmental parameters of SwellEx-96 are used in this experiments [22]. As shown in Fig. 3, the topmost layer is water with a depth of 216.5 meters and a density of 1g/m$^2$. The seafloor first consists of a 23.5m thick layer of sediment with a density of 1.76g/m$^2$ and a decay of 0.2dB/mkHz. The sound speed at the top of the sedimentary layer is 1572.368m/s, and the sound speed at the bottom is 1593.016m/s. At the bottom is a 800m-thick mudstone layer with a density of 2.06g/m$^2$ and a attenuation of 0.06dB/mkHz. The upper and lower speed of mudstone is 1881m/s and 3245m/s, respectively. At the bottom is an infinite half space with a density of 2.66g/s, an attenuation of 0.020dB/mkHz, and a sound speed of 5200m/s.

### B. Marine Data Processing

The SwellEx-96 experiment includes S5 and S59 experiments. We use the S5 experimental data. The test sound source of S5 is dragged at the speed of 2.5m/s at the depth of 54m for 75 minutes. The sound source randomly selects 13 frequencies between 49Hz and 388Hz, and the hydrophone array contains 21 hydrophones. The depth of each hydrophone is shown in Table I. In this test, the 75-minute data are processed, and the signal frequency is 388Hz. The sound field is considered to be independent of the distance, and the kraken normal wave model is used for calculation acoustic field [15]. The matching method adopts the minimum mean square error method. The signal sampling frequency at the hydrophone is 1500Hz. The first 1s data are matched. The experimental results are shown in Fig. 4.

In Fig. 4, the horizontal axis represents the time (minutes), and the vertical axis represents the horizontal distance matching result. The curve with sign $o$ represents the matched sound source trajectory, and the curve with sign $*$ represents the motion trajectory of the actual sound source. Obviously there is a large error in the matching result.

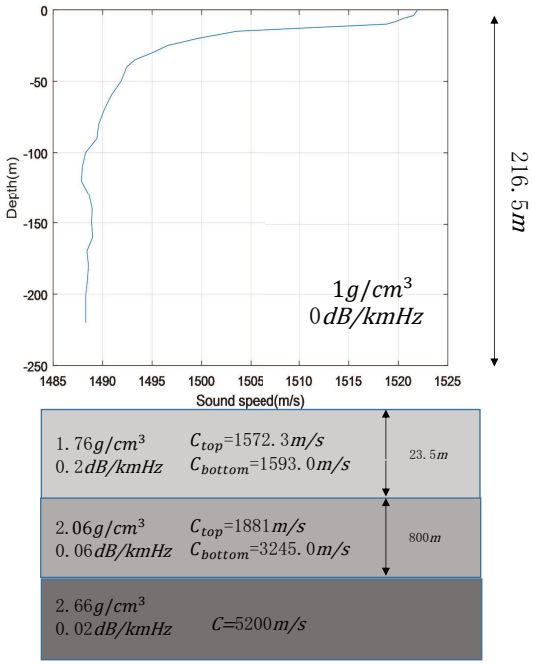


Fig. 3. Experimental Environment.

Because there is only a single vertical array in this experiment, the positioning results of the same array at different times are used to replace the positioning results of different arrays at the same time, and then the positioning results are fused. The number of hydrophones in each sub-array of multiple arrays is the same as that in the single array. The positioning results are shown in Fig. 5.

Fig. 5 shows average positioning result error with respect to the number of hydrophones. It is observed that the overall positioning result error decreases with the increase of the number of hydrophones, and the average error with two arrays is around 400-600m which is less than that of single array positioning.

TABLE I. Hydrophone Index Number and Depth

| Element Number | Depth(m) | Element Number | Depth(m) |
|---|---|---|---|
| 1 | 212.25 | 34 | 150.38 |
| 4 | 206.62 | 37 | 144.74 |
| 7 | 200.99 | 40 | 139.12 |
| 10 | 195.38 | 46 | 127.88 |
| 13 | 189.76 | 49 | 122.25 |
| 16 | 184.12 | 52 | 116.62 |
| 19 | 178.49 | 55 | 111.00 |
| 22 | 172.88 | 58 | 105.38 |
| 25 | 167.26 | 61 | 99.755 |
| 28 | 161.62 | 64 | 94.125 |
| 31 | 155.99 | | |

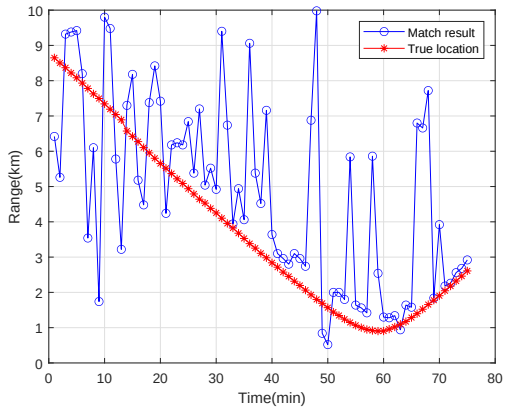


Fig. 4. 75-min Horizontal Distance Matching Results.

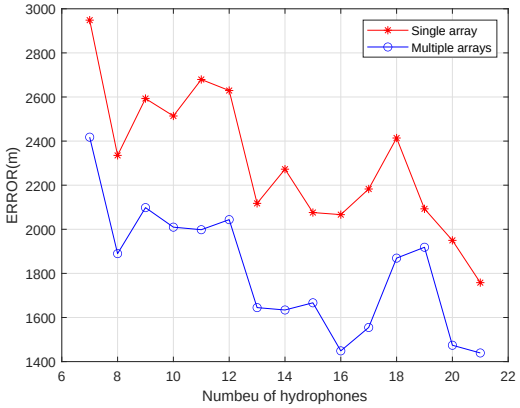


Fig. 5. The Average Positioning Error Varies with the Number of Hydrophones.

### *C. Simulation for Performance Comparison of The Single Array and Multiple Sub-array System*

The environment for the SwellEx-96 experiment is relatively ideal, and it is with low noise, high transmission power and high *SNR*. Thus in such situation the advantages of multiple arrays are not obvious. To verify the performance of the algorithm in low *SNR*, instead of experimental data, we use simulation data to evaluate the positioning error by dynamically varying the noise power.

The signal transmitting frequency is 388Hz. The sound field is considered to be independent of the distance. The normal mode is used to calculate acoustic field, and the kraken is used to calculate the acoustic field [15]. A single hydrophone array consists of 20 hydrophones, ranging from 94.125 meters to 206.62 meters in depth. Set $\boldsymbol{x}_R = (r_0, h_0) = (3000m, 60m)$. In the simulation, the horizontal search range is 0-10km, and the step size is 20m; The vertical search interval is 0-100m and the step length is 2m. Then the 20 hydrophones are divided into four groups, and each group has five hydrophones, called sub-array, which are located in the same depth as that of the first five hydrophones of the single hydrophone array. The horizontal distance between sub-arrays and the sound source are $r_1 = 1km$, $r_2 = 3km$, $r_3 = 7km$ and $r_4 = 8km$, respectively. The positioning error is defined as the Euclidean distance between the estimated position and the true one, i.e., $E_R = \sqrt{(r_m - r_0)^2 + (h_m - h_0)^2)}$, where $(r_m, h_m)$ is the estimated position. Since $(r_m, h_m)$ represents the center point of the matching position, when the positioning error is less than the search step, the positioning error is regarded as 0. The received *SNR* is defined as $SNR = 10\log_{10}\frac{P_s \sum_{i=1}^{N} |g_i(x)|^2/N}{\sigma^2}$, where $P_s$ is the power of the signal source, and $\sigma^2$ is the noise power. For the multiple sub-array system, different sub-arrays are placed at different locations, and the signal array system is placed in a different location. Considering the sound wave directivity, we assume the transmission power of sound source for the signal array system is $P_{s,0}$, and the transmission power of sound source for a sub-array is $P_{s,k}, k = 1, 2, \cdots, 4$. Set $P_{s,0}$=0.65W, $P_{s,1} = 0.25W, P_{s,2} = 0.5W, P_{s,3} = 0.75W$, and $P_{s,4} = 0.1W$, respectively. Four hydrophone sub-arrays are used to localize the sound source independently, and the final localization results are fused to determine the location of sound source. The mean value of noise is 0W, and the standard deviation is $\sigma = 0.001 - 0.01$W. With 5000 trials, the positioning results are shown in Fig. 6.

From Fig. 6, when the *SNR* is between -5dB and -19dB, the positioning error of the single array is 0, and this proves that low noise power has slight influence on the positioning result of the single array. The positioning error of multiple sub-arrays increases from 11m to 60m. Obviously the positioning error of multiple sub-arrays is higher than that of single arrays. However, when the *SNR* is between -25dB and -21dB, the positioning error of the single array system increases rapidly when the *SNR* decreases, which is from 3m to 124m. The positioning error of multiple arrays increases slowly from 65m to 67m.

Set $\sigma = 0.01 - 0.1$. The average positioning errors with respect to *SNR* are shown in Fig. 7. It is observed that the positioning error does not increase with the decrease of *SNR*, and there is a threshold effect in the positioning result. The positioning error of the single array remains around 145m after -30dB, while the positioning error of the multiple sub-arrays remains around 67m, which is 78m less than that of the single array. With low *SNR*, the positioning accuracy of the multiple sub-arrays is much higher than that of the single array.

When the number of hydrophones is set to 15, the positioning results of the single array and multiple sub-arrays are shown in Fig. 8. It is observed that the positioning error of the

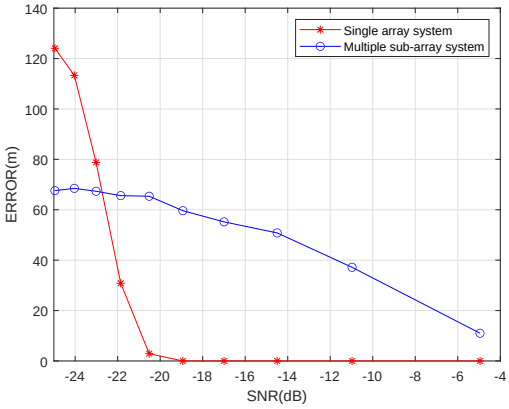


Fig. 6. When $SNR = -25 \sim -5dB$, the Positioning Errors of the Single Array System with 20 Hydrophones and the Four Sub-arrays, Each with 5 Hydrophones.

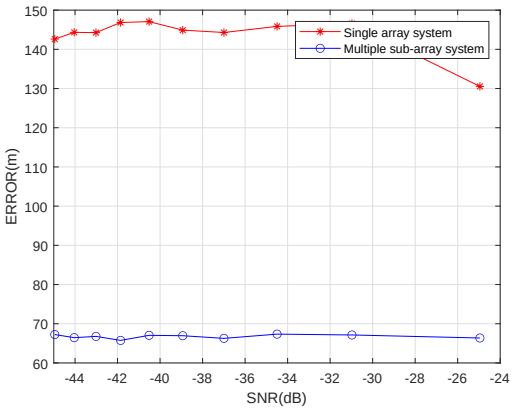


Fig. 7. When $SNR = -46 \sim -25dB$, the Positioning Errors of the Single Array System with 20 Hydrophones and the Four Sub-arrays, Each with 5 Hydrophones.

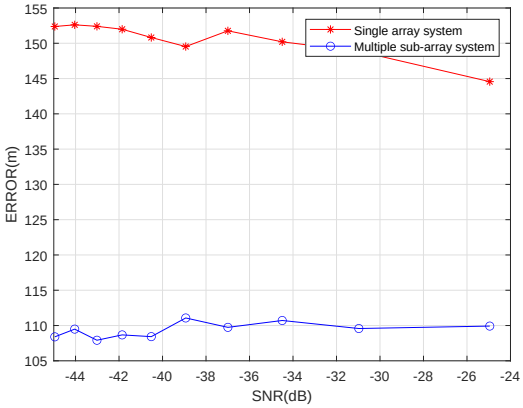


Fig. 8. When $SNR = -46 \sim -25dB$, the Positioning Errors of the Single Array System with 15 Hydrophones and the Three Sub-arrays, Each with 5 Hydrophones.

single array is about 151m and that of multiple sub-arrays is about 109m. Hence, when 5 hydrophones are added, the single array positioning error is reduced by 6m, while the multiple sub-array positioning error is reduced by 42m, which shows that the multiple sub-array positioning accuracy is improved significantly.

The effect of the number of hydrophones in each hydrophone array on the positioning accuracy is shown in Fig. 9. Set $\sigma = 0.1$ and $m = 1$. The average positioning error decreases with the number of hydrophones. When the number of hydrophones changes from 5 to 10, the positioning error decreases with a higher rate, whereas when the number of hydrophones changes from 10 to 20, the positioning error decrease with a slower rate. Note that, $E(N)$ jumps to a higher value when the number of hydrophones is 12, 13 and 16, respectively, in that situation the hydrophones are in a high noisy environment and the positioning accuracy decreases.

### *D. Simulation for Optimal Structure of Multiple Sub-arrays*

To find the optimal number of hydrophones in each sub-array for high-accuracy positioning, 20 hydrophones are divided into multiple groups to form different sub-array structures which are decided by the number of hydrophones in each sub-array and the total number of sub-arrays. Each hydrophone

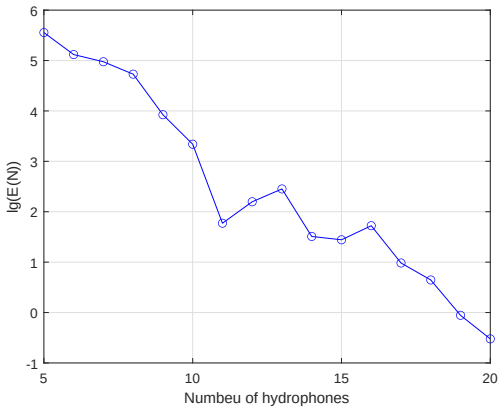


Fig. 9. When the $\sigma = 0.1$, the $\log_{10} E(N)$ Changes with the Number of Hydrophones.

sub-array contains at least 5 hydrophones. Herein we consider 4 sub-array structures to verify the positioning performance. Structure 1: the structure of sub-arrays is same as that defined in Section V-C; Structure 2: The 20 hydrophones are divided into two sub-arrays, and each array has 10 hydrophones. Set $P_{s,0} = 0.75W$, $P_{s,1} = 0.5W$ and $P_{s,2} = 1$, respectively. Set $r_1 = 3km$ and $r_2 = 8km$, respectively, where $r_j$ represents the horizontal distance between the $j$th sub-array and the sound source; Structure 3: 20 hydrophones are divided into 3 sub-arrays, and the number of hydrophones in each array is 6, 7, and 7, respectively. Set $P_{s,0} = 0.725W$, $P_{s,1} = 0.5W$, $P_{s,2} = 0.75W$, and $P_{s,3} = 1W$, respectively. Set $r_1 = 3km$, $r_2 = 7km$, and $r_3 = 8km$, respectively; Structure 4: 20 hydrophones are divided into 3 sub-arrays, and the number of hydrophones in each array is 6, 6, and 8, respectively. Set $P_{s,0} = 0.775W$, $P_{s,1} = 0.5W$, $P_{s,2} = 0.75W$, and $P_{s,3} = 1W$ respectively. Set $r_1 = 3km$, $r_2 = 7km$, and $r_3 = 8km$, respectively. The positioning results of multiple sub-arrays for Structure 2-4 and the corresponding positioning results of the single array are shown in Fig. 10-15.

Let $E_{rs}$ represent the average positioning error of the single array and $E_{rm}$ represent the average positioning error of multiple sub-arrays. From Fig. 10 and Fig. 11, when the *SNR* is less than -30dB, $E_{rs}$ is around 145m, while $E_{rm}$ is around 97m. The positioning error of the multiple sub-arrays

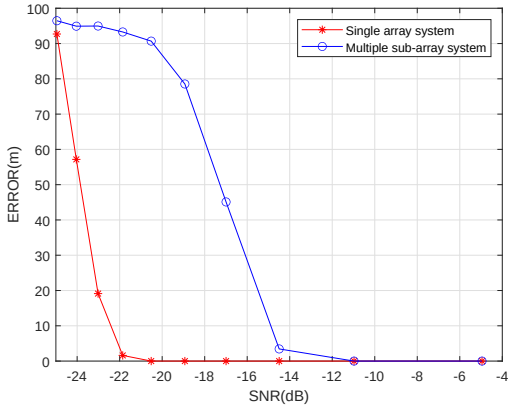


Fig. 10. When $SNR = -25 \sim -5dB$, the Positioning Results of the Single Array System and Multiple Sub-array System of Structure 2.

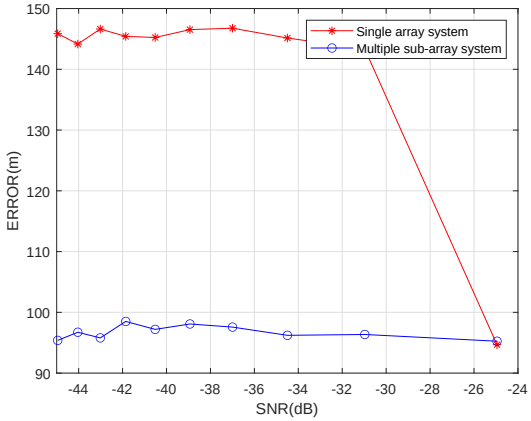


Fig. 11. When $SNR = -46 \sim -25dB$, the Positioning Results of the Single Array System and Multiple Sub-array System of Structure 2.

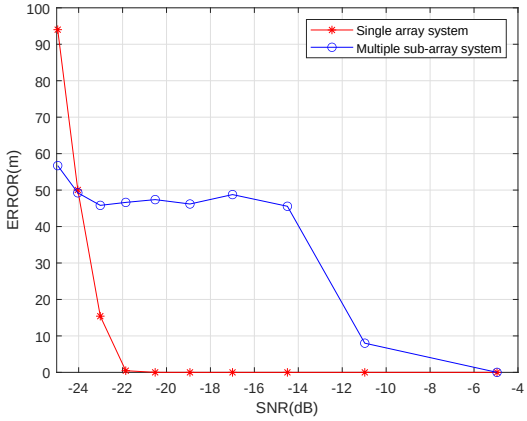


Fig. 12. When $SNR = -25 \sim -5dB$, the Positioning Results of the Single Array System and Multiple Sub-array System of Structure 3.

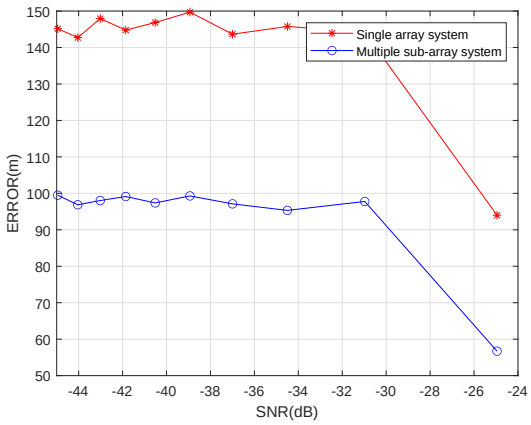


Fig. 13. When $SNR = -46 \sim -25dB$, the Positioning Results of the Single Array System and Multiple Sub-array System of Structure 3.

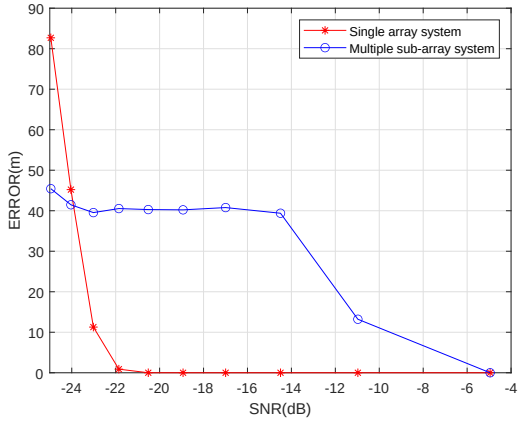


Fig. 14. When $SNR = -25 \sim -5dB$, the Positioning Results of the Single Array System and Multiple Sub-array System of Structure 4.

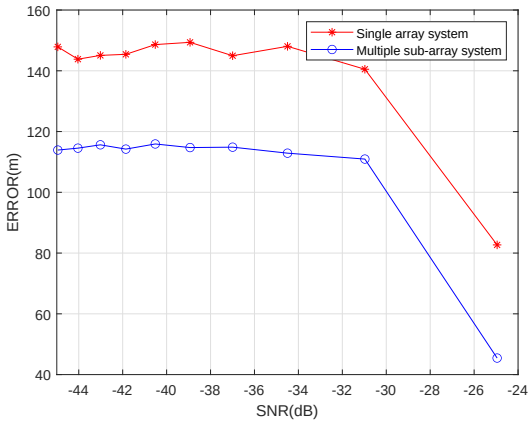


Fig. 15. When $SNR = -46 \sim -25dB$, the Positioning Results of the Single Array System and Multiple Sub-array System of Structure 4.

is 48m less than that of the single array. For the Structure 3, $E_{rs}$ is around 146m, and $E_{rm}$ is around 98m. For the Structure 4, $E_{rs}$ is around 146m and $E_{rm}$ is around 114m. In summary, for the positioning errors produced by the four structures, $E_{rm,1} < E_{rm,2} < E_{rm,3} < E_{rm,4}$, where $E_{rm,k}$ is the positioning error produced by Structure $k$. With the configured parameters of the four structures, the numerical results $\hat{E}_{rm,k}$ yielded by (18) are $\hat{E}_{rm,1} = 4.32$, $\hat{E}_{rm,2} = 7.62$, $\hat{E}_{rm,3} = 8.08$, and $\hat{E}_{rm,4} = 9.35$, respectively, and $\hat{E}_{rm,1} < \hat{E}_{rm,2} < \hat{E}_{rm,3} < \hat{E}_{rm,4}$. Those are consistent with the simulation results. Hence, under the current experimental conditions, when the *SNR* is lower than -30dB, the Structure 1 achieves the highest positioning accuracy.

## VI. Conclusion

The experimental results show that when the *SNR* is higher than a threshold, the positioning error of the multiple sub-array system is slightly higher than that of the single array system. However, when the *SNR* decreases, the positioning error of the single array decreases faster than that of the multiple sub-array system, and will exceeds that of the multiple sub-array system. When the *SNR* reduces to a certain threshold, the positioning error will not increase with the decrease of *SNR*, and the positioning error of the single array system is around twice

that of the multiple sub-array system. In addition, by designing different multiple sub-array structures, the simulation results of positioning errors of the multiple sub-array system are obtained, and they are consistent with the theoretical analysis.

In this paper, a multiple sub-arrays joint positioning method is proposed based on the MFP technology. Assume the total number of hydrophones remains unchanged, a single hydrophone array is divided into multiple hydrophone sub-arrays for independent positioning, and the positioning results of sub-arrays are fused to obtain the sound source location. Average positioning error of the multiple hydrophone sub-array system is derived and then the number of sub-arrays and the number of hydrophones in each sub-array are discussed. Experiments and simulations show that the multiple sub-array system can improve the positioning accuracy compared with the single hydrophone array in the noisy environment. The average positioning errors produced by the experiments are consistent with the numerical ones based on the derived formula.

## ACKNOWLEDGMENT

This research did not receive any specific grant from funding agencies in the public, commercial or nonprofit sectors. My sincere acknowledgment goes to Dr. Li Xiukui.

## REFERENCES

[1] Clay, C.S. Use of arrays for acoustic transmission in a noisy ocean. Reviews of Geophysics. 4(4), 475–507, 1966.

[2] Hinich, M.J. Maximum likelihood estimation of the position of a radiating source in a waveguide. The Journal of the Acoustical Society of America. 66(2), 480–483, 1979.

[3] David, R. Dowling, R. Incomplete acoustic time reversal, frequency shifting, and matched field processing. The Journal of the Acoustical Society of America. 150, A193-A193, 2021. https://doi.org/10.1121/10.0008096

[4] Scripps, UCSD, L.A., Jolla, C.A. Localizing a quiet moving source with range-coherent matched field processing. The Journal of the Acoustical Society of America. 150, A277-A277, 2021. https://doi.org/10.1121/10.0008283

[5] Capon, J., Greenfield, R.J., Kolker, R.J. Multidimensional maximum-likelihood processing of a large aperture seismic array. Proceedings of the IEEE. 55(2), 192–211, 1967.

[6] Tran, P.N., Trinh, K.D. Adaptive matched field processing for source localization using improved diagonal loading algorithm. Acoust Aust. 45, 325–330, 2017. https://doi.org/10.1007/s40857-017-0089-4

[7] Shang, E.C. Source depth estimation in waveguides. The Journal of the Acoustical Society of America. 77(4), 1413–1418, 1985.

[8] Shang, E.C., Clay, C.S., Wang, Y.Y. Passive harmonic source ranging in waveguides by using mode filter. The Journal of the Acoustical Society of America. 78(78), 172–175, 1985.

[9] Yang, T.C. A method of range and depth estimation by modal decomposition. The Journal of the Acoustical Society of America. 82(5), 1736–1745, 1987. .

[10] Yang, T.C. Effectiveness of mode filtering: A comparison of matched-field and matched-mode processing. The Journal of the Acoustical Society of America. 87(5), 2072–2084, 1987.

[11] Battle, D.J., Gerstoft, P., Hodgkiss, W.S. Bayesian model selection applied to self-noise geoacoustic inversion. The Journal of the Acoustical Society of America. 116(4), 2043–2056, 2004.

[12] Debever, C. Investigation of the Limits of Broadband Robust Matched-field Processing. University of California, San Diego, 2011.

[13] Collins, M.D., Makris, N.C., Fialkowski, L.T. Noise cancellation and source localization. The Journal of the Acoustical Society of America. 96(3), 1773–1776, 1994.

[14] Lee, Y.P. Multiple-frequency robust adaptive matched-field processing(mfp) in shallow water. The Journal of the Acoustical Society of America. 97(5), 3290–3290, 1995.

[15] Song, H.C., Seong, W. Localization of a moving source in oceanic waveguide using a vertical array in the presence of correlated noise. The Journal of the Acoustical Society of America. 95(5), 2981–2981, 1994.

[16] Nicholas, M., Perkins, J.S., Orris, G.J.: Source motion mitigation for adaptive matched field processing. The Journal of the Acoustical Society of America. 113, 2719–2731, 2003. https://doi.org/10.1121/1.1561817

[17] Zurk, L.M., Lee, N., Ward, J. Environmental inversion and matched-field tracking with a surface ship and an l-shaped receiver array. The Journal of the Acoustical Society of America. 116, 2891–2901, 2004. https://doi.org/10.1121/1.1802755

[18] Tollefsen, D., Gerstoft, P., Hodgkiss, W.S. Multiple-array passive acoustic source localization in shallow water. The Journal of the Acoustical Society of America. 141(3), 1501–1501, 2017.

[19] Tracey, B.H. Statistical description of matched field processing ambiguity surfaces. The Journal of the Acoustical Society of America. 118, 1372–1380, 2005. https://doi.org/10.1121/1.2000750

[20] Bogart, Christopher, W. Source localization with horizontal arrays in shallow water: Spatial sampling and effective aperture. The Journal of the Acoustical Society of America. 96(3), 1677–1686, 1994.

[21] Tantum, S.L., Nolte, L.W. On array design for matched-field processing. The Journal of the Acoustical Society of America. 107, 2101–2101, 2000. https://doi.org/10.1121/1.428492

[22] Murray, J., Ensberg, D. The swellex-96 experiment[eb/ol], 1996. figshare http://swellex96.ucsd.edu/